

Spin relaxation properties in graphene due to its linear dispersion

Sanghyun Jo,^{1,*} Dong-Keun Ki,^{1,*} Dongchan Jeong,¹ Hu-Jong Lee,^{1,†} and Stefan Kettmann^{2,3}

¹*Department of Physics, Pohang University of Science and Technology, Pohang 790-784, Republic of Korea*

²*Division of Advanced Materials Science, Pohang University of Science and Technology, Pohang 790-784, Republic of Korea*

³*School of Engineering and Science, Jacobs University Bremen, Bremen D-28759, Germany*

(Received 12 June 2011; published 10 August 2011)

A spin injection is achieved in a direct-contact cobalt–single-layer graphene nonlocal spin-valve system, overlaid with a top gate. The spin signal is retained even in bipolar configurations of graphene. Hanle spin-precession analysis demonstrates that proportionality between spin and momentum relaxation times, which supports the Elliot-Yafet-type spin relaxation, holds consistently only when the carrier-density dependence of the density of states is taken into account. The corresponding strong spin-orbit coupling (~ 10 meV) suggests that covalently bonded adsorbates, rather than charged impurities, govern the spin relaxation in diffusive graphene.

DOI: [10.1103/PhysRevB.84.075453](https://doi.org/10.1103/PhysRevB.84.075453)

PACS number(s): 75.76.+j, 72.80.Vp, 75.70.Tj

I. INTRODUCTION

Graphene shows gate-tunable spin transport and potentially long spin-relaxation time arising from weak intrinsic spin-orbit (SO) interaction. In addition, the spin coherence in graphene survives up to unusually high temperatures. These unique features make graphene highly promising for spintronic applications. However, observed spin-relaxation time and length in diffusive graphene^{1–8} are far shorter than theoretical estimations based on the weak SO interaction.^{9–12} It is believed that the interplay between extrinsic momentum relaxation and SO coupling via Elliot-Yafet (EY) and/or D'yakonov-Perel (DP) mechanisms¹³ are responsible for the enhanced spin relaxation in diffusive graphene.^{5–10,14}

Recent studies on the role of momentum scattering by charged impurities in spin relaxation indicates that pristine graphene favors the EY spin-relaxation mechanism^{5–7} while the spin relaxation in graphene doped with charged Au impurities can be due to the DP mechanism.⁸ However, this is in contrast to the fact that the EY mechanism is known to be predominant in systems with more momentum scatterers such as charged impurities.¹³ Thus, it is of prime importance to find the exact cause of the enhanced spin-relaxation rate and clarify the SO mechanism that is responsible for the spin relaxation in this material in a diffusive limit.

We infer that covalently bonded monovalent adsorbates on graphene may cause the enhanced spin relaxation. A first-principle calculation demonstrated that the distortion of the graphene lattice by sp^3 hybridization of adsorbates with carbon atoms induces a strong SO coupling,¹⁰ on the order of 1 meV. This can lead to a high spin-relaxation rate, which is hardly attained by charged impurities.¹⁴

We report spin-injection measurements in a direct-contact cobalt–single-layer-graphene nonlocal spin-valve system, overlaid with a top gate. No additional spin relaxation was observed as the carriers traversed the interface, particularly for the bipolar configuration of graphene. The spin relaxation for a homogeneous graphene configuration with neutral top gate was also studied via measurements of the Hanle spin-precession effect. Hanle analysis demonstrated that the ratio between spin and momentum relaxation times is proportional to the square of the density of states, which varies with

the carrier density due to the unique linear dispersion relation of graphene.¹⁵ This behavior was recently predicted theoretically in graphene in association with the EY spin-relaxation mechanism⁹ but has been overlooked in previous experimental studies.^{5–8,16} Based on this relationship leading to the EY-type spin relaxation, we determined SO coupling to be ~ 9 – 10 meV, seemingly suggesting that a local distortion of the graphene lattice by sp^3 -bonded adsorbates dominated the spin relaxation.¹⁰

II. SAMPLE FABRICATION AND MEASUREMENT CONDITIONS

In our device, we enhanced the spin-injection efficiency by reducing the contact area or, equivalently, by increasing the spin-flip resistance in the ferromagnet.^{2,17,18} A nanoribbon of graphene (200 nm wide) was used to reduce the ferromagnet–graphene contact area rather than partially masking the graphene layer in direct contact with the cobalt layer, as used by Han *et al.*² Our configuration provided the freedom to easily place a top gate on graphene, allowing examination of the spin relaxation through a p-n-type potential-varying interface that forms at an edge of the top gate. It also allows variation of the carrier density without changing the doping level of graphene underneath the electrodes.

Figure 1(a) schematically illustrates the sample geometry. A 0.2 - μm -wide graphene nanoribbon was exfoliated from natural graphite onto the SiO_2/Si substrate. The electrodes were patterned using electron-beam lithography, following spin-coating of a single layer of PMMA 950K C4 on the substrate. Then, electrodes, each consisting of a 50 -nm-thick Co ferromagnet layer and a 5 -nm-thick Au protection layer, were electron-gun (e-gun) deposited directly on graphene. Both the injector and detector electrodes were 0.11 μm wide, leaving a contact area of 0.022 μm^2 . The spacing (L) between the injector and the detector was 2 μm . A Ti/Au (5 nm/ 55 nm) bilayer top gate was then e-gun deposited to cover half of the graphene layer, where a cross-linked PMMA layer was placed to electrically insulate the top gate from graphene. No annealing was taken in the entire sample fabrication process. The electrical and spin transports were

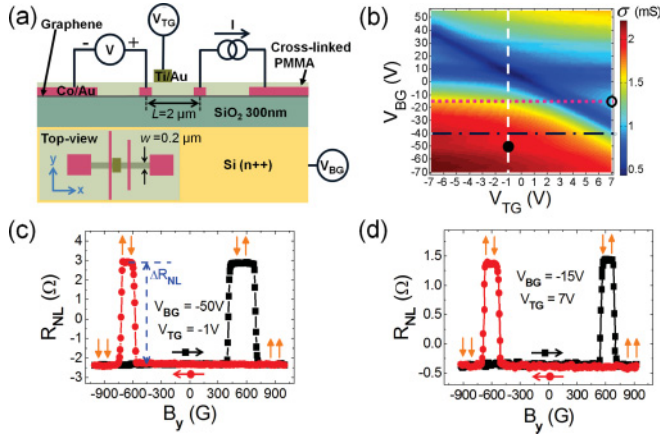


FIG. 1. (Color online) (a) Nonlocal measurement configuration and its top view (inset). (b) Quadrant conductivity map for varying V_{BG} and V_{TG} . Nonlocal magnetoresistance (R_{NL}) for varying magnetic fields B_y in the y -direction (c) at $V_{BG} = -50$ V and $V_{TG} = -1$ V [filled circle in (b)] and (d) at $V_{BG} = -15$ V and $V_{TG} = 7$ V [void circle in (b)] for opposite field-sweeping directions.

measured at 4.2 K, using a standard ac lock-in technique ($f = 13.3$ Hz) in a bias level of $10 \mu\text{A}$ rms, in standard four-probe local and nonlocal configurations, respectively. The scheme for the nonlocal measurements is illustrated in Fig. 1(a). The single-layered structure of graphene was confirmed by quantum-Hall measurements. The electrical mobilities at 4.2 K were around $4,000 \text{ cm}^2\text{V}^{-1}\text{s}^{-1}$, indicating the diffusive nature of the adopted graphene.

III. EXPERIMENTAL RESULTS AND ANALYSIS

A. Gate-voltage dependence of spin signal

Figure 1(b) shows the quadrant conductivity (σ) map for varying back-gate (V_{BG}) and top-gate (V_{TG}) voltages.¹⁹ In the two gating conditions denoted by filled and void circles in Fig. 1(b), nonlocal magnetoresistance (R_{NL}) was measured while sweeping magnetic fields in the y direction [inset of Fig. 1(a)]. In Fig. 1(c), measured R_{NL} shows a clear spin-valve signal for $V_{BG} = -50$ V and $V_{TG} = -1$ V (filled circle), where the top-gate was set to be neutral to attain the homogeneous state of the graphene layer. A clear spin signal also developed for $V_{BG} = -15$ V and $V_{TG} = 7$ V (void circle) as shown in Fig. 1(d), where the spin current was across the bipolar state of the graphene layer.

Figure 2(a) shows the evolution of the spin signal (ΔR_{NL}) with varying V_{BG} for a fixed $V_{TG} (= -1$ V) [along the vertical dashed line in Fig. 1(b)], where ΔR_{NL} is defined in Fig. 1(c). In contrast to previous results,⁴ a strong correlation between ΔR_{NL} and σ was not observed. As demonstrated by Takahashi *et al.*,¹⁷ in the “intermediate contact regime,” ΔR_{NL} is sensitive to the contact resistance between graphene and the injector and/or detector electrodes. In our study, changes in the contact resistance for varying V_{BG} , a common feature in direct-contact metal–graphene systems,²⁰ was traced [Fig. 2(d)]. With our contact resistances in the intermediate regime,²¹ we attribute the weak correlation between ΔR_{NL} and σ to the V_{BG} -induced variation of the contact resistance.

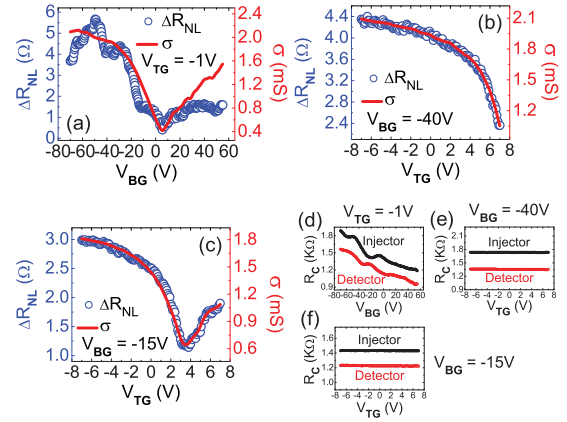


FIG. 2. (Color online) Evolution of the spin signal (ΔR_{NL}) and the conductivity (σ) for (a) varying V_{BG} at $V_{TG} = -1$ V, (b) varying V_{TG} at $V_{BG} = -40$, and (c) varying V_{TG} at $V_{BG} = -15$ V. Variations in the contact resistances of the injector and the detector electrodes for the conditions in (a), (b), and (c) are shown in (d), (e), and (f), respectively.

In contrast with Fig. 2(a), variations in ΔR_{NL} and σ are strongly correlated with each other for varying V_{TG} along the horizontal dash-dotted line in Fig. 1(b) at $V_{BG} = -40$ V [see Fig. 2(b)]. The difference arose because, unlike V_{BG} , V_{TG} does not affect the condition of the junction area underneath the electrodes, leaving the junction contact resistance intact, as illustrated in Figs. 2(e) and 2(f). ΔR_{NL} scales with σ , even in the presence of the potential-varying interface near an edge of the top gate, with the electric field becoming stronger as V_{TG} moved further from -1 V. In Fig. 2(c), similar scalability between ΔR_{NL} and σ is seen as V_{TG} varies between -7 and 7 V for $V_{BG} = -15$ V [along the horizontal dotted line in Fig. 1(b)]. The high quality of the scalability is retained, even deep into the bipolar state of the graphene layer, which formed for $V_{TG} > 3.5$ V. Thus, the top gate provides a convenient means to precisely control the spin signal via the gate-induced change in conductivity.

In graphene, the Rashba-type SO interaction induced by the electric field is predicted to be weak due to weak atomic SO interactions,^{11,12} which may explain the robust scalability between ΔR_{NL} and σ , even in the presence of the potential-varying interface, in our diffusive graphene around 4.2 K. In particular, the robustness of the scalability to the formation of a bipolar configuration may indicate that Klein tunneling does not further relax spins. For more detailed analysis see Section IV.

B. Hanle effect analysis

Figure 3 shows spin relaxation results using the Hanle effect along the dashed line in Fig. 1(b) for the neutral top gate. The symmetric part of the Hanle signal for $V_{BG} = -50$ V and $V_{TG} = -1$ V [filled circle in Fig. 1(b)] with varying magnetic fields B_n normal to the xy plane is shown in Fig. 3(a). Here, θ_1 (θ_2) is the possible tilt angle of the injector (detector) magnetization from the y direction to the B_n direction. The Hanle signal deduced from $R_{\text{Hanle}}(\theta_{1,2})$ in Fig. 3(a) for $\theta_{1,2} = 0$ is shown in Fig. 3(b).^{5,22}

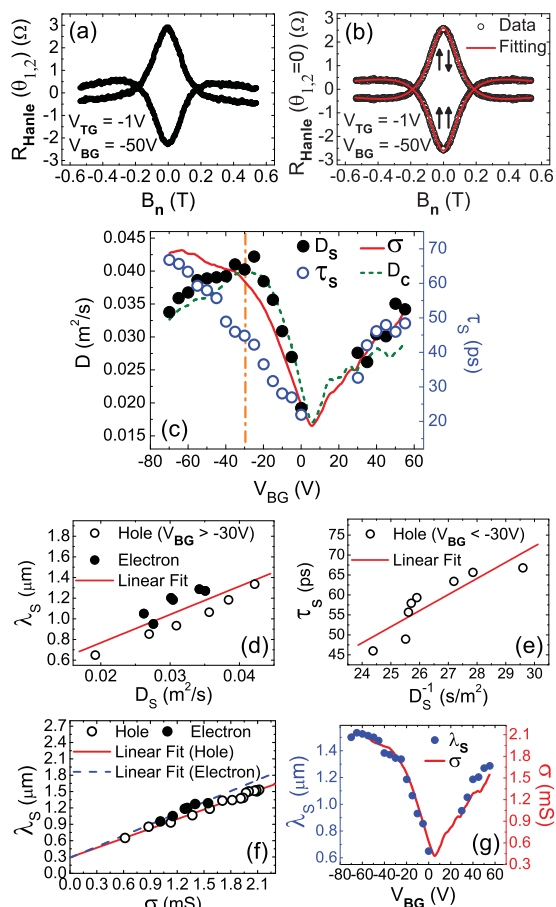


FIG. 3. (Color online) Hanle analysis for varying V_{BG} at $V_{TG} = -1$ V. (a) The symmetric part of the Hanle signal [$R_{Hanle}(\theta_{1,2})$] for $V_{BG} = -50$ V and $V_{TG} = -1$ V with varying B_n . θ_1 (θ_2) is the possible tilt angle of the injector (detector) magnetization relative to the direction of B_n . (b) Hanle signal for $\theta_{1,2} = 0$. (c) The spin diffusion constant (D_s) and the spin-relaxation time (τ_s) extracted from the best fits of Hanle signals, along with the charge diffusion constant (D_c) and σ . (d) λ_s ($=\sqrt{D_s \tau_s}$) vs. D_s in the hole and electron sides and the linear fit for $V_{BG} > -30$ V. (e) τ_s vs. D_s^{-1} and the linear fit for $V_{BG} < -30$ V. (f) λ_s in the hole and electron sides for varying σ and the linear fits in the corresponding ranges of V_{BG} . (g) Variations in λ_s and σ vs V_{BG} .

The best fit of $R_{Hanle}(\theta_{1,2} = 0)$ to Eq. (1) with 95% confidence is also denoted in Fig. 3(b).

$$R_{Hanle}^{P(AP)} = \mp A \int_0^\infty \frac{1}{\sqrt{4\pi D_s t}} e^{-L^2/(4D_s t)} \cos(\omega_L t) e^{-t/\tau_s} dt. \quad (1)$$

Here, A is amplitude, which depends on the polarization and the density of states, D_s is the spin diffusivity, ω_L ($=g\mu_B B_n/\hbar$) is the Larmor frequency, P(AP) stands for the parallel (antiparallel) configuration between injector and detector magnetization, and $-(+)$ corresponds to P(AP). D_s and τ_s are extracted from the best fits of $R_{Hanle}(\theta_{1,2} = 0)$ for varying V_{BG} along the dashed line in Fig. 1(b). The result is plotted along with the carrier diffusivity (D_c) and σ in Fig. 3(c). Here, D_c is obtained from the relationship⁶ of $D_c = \sigma/(e^2 \nu^*)$. To avoid a singularity of D_c around the

charge-neutral point, the Gaussian-broadened density of states ν^* is obtained by considering the density fluctuation⁶ as $\nu^*(E) = \frac{1}{\sqrt{2\pi\alpha}} \int_{-\infty}^\infty \exp(-\frac{(\epsilon-E)^2}{2\alpha^2}) \nu(\epsilon) d\epsilon$. Here, ν is the unbroader density of states and α is the energy broadening. D_c in Fig. 3(c) is for $\alpha = 130$ meV, and the full-width-at-half-maximum of the corresponding density fluctuation of $\Delta n \approx \pm 1.7 \times 10^{12}$ cm⁻². As noted by Jozsa *et al.*,⁶ D_s and D_c are almost identical to each other. The most notable feature in Fig. 3(c) is that, unlike τ_s , D_s varies nonmonotonously near $V_{BG} = -30$ V (dash-dotted line). Both D_s and τ_s increase with increasing carrier density for $V_{BG} > -30$ V, while D_s (τ_s) decreases (increases) for $V_{BG} < -30$ V. The evolution of σ also changes around $V_{BG} = -30$ V, where a conspicuous sublinearity develops for $V_{BG} < -30$ V.

λ_s ($=\sqrt{D_s \tau_s}$) vs. D_s is plotted in Fig. 3(d), for $V_{BG} > -30$ V. The relationship between λ_s and D_s indicates a proportionality between τ_s and the momentum-relaxation time (τ_m), which is strong evidence of the EY spin-relaxation mechanism observed in semiconductors and metals.¹³ Recent experimental studies on graphene have also demonstrated similar findings.⁵⁻⁷

Figure 3(e), however, exhibits a proportionality between τ_s and D_s^{-1} for $V_{BG} < -30$ V, implying an inverse proportionality between τ_s and τ_m . This relationship, in contrast to that of Fig. 3(d), may signify the DP spin-relaxation mechanism.¹³ Thus, judging solely from the relationship between τ_s and τ_m , the spin-relaxation mechanism appears to change with varying carrier density. However, more careful analysis leads to a different conclusion.

As shown in Fig. 3(f), a linear relationship exists between λ_s and σ over the entire range of V_{BG} . The linearity is also supported by the conformable variation of λ_s and σ vs V_{BG} in Fig. 3(g). Using the Einstein relation ($\sigma = e^2 D \nu$), the linearity between λ_s and σ results in

$$\tau_s \propto \nu^2 \tau_m, \quad (2)$$

where we set $D = D_c = D_s$. Recent theoretical work by Huertas-Hernando *et al.*⁹ demonstrated that the EY spin-relaxation mechanism in graphene leads to

$$\tau_s \approx \frac{E_F^2}{\Delta_{SO}^2} \tau_m, \quad (3)$$

where E_F is the Fermi energy and Δ_{SO} is the SO coupling constant. Because a linear relationship between ν and E_F exists in graphene, Eq. (3) coincides with Eq. (2), meaning that the EY mechanism holds in our graphene in the entire range of V_{BG} . In previous experimental studies on graphene,⁵⁻⁸ the spin relaxation mechanism has been investigated in terms of the relationship between τ_s and τ_m . However, the relationship in Fig. 3(e), without accounting for the V_{BG} dependence of ν^2 , can lead to an erroneous conclusion for the spin-relaxation mechanism. Despite recent reports on other possible causes of spin relaxation,^{4,7-9,14} our study indicates that the EY mechanism governs spin relaxation in graphene in the diffusive regime.

The SO couplings (Δ_{SO}), obtained by direct comparison between the slopes of linear fits in Fig. 3(f) and the prefactor in Eq. (3), are 10.3 and 8.8 meV in the hole and electron

sides, respectively. The nonzero intercepts in the linear fits, resulting from the finite minimum conductivity, do not affect this analysis. In general, σ is expressed²³ as $\sigma = \sigma(n) + \sigma_{\min}$, where $\sigma(n)$ is the conductivity depending on the carrier density n and σ_{\min} is the n -independent finite minimum conductivity. Thus, Eq. (3) is equivalent to the relation

$$\lambda_s \approx a\sigma = a\sigma(n) + a\sigma_{\min}, \quad (4)$$

where a is a prefactor and is inversely proportional to Δ_{SO} . The second term, $a\sigma_{\min}$, corresponds to the nonzero intercept in the linear fit in Fig. 3(f). Using the measured value of σ_{\min} (=0.440 mS) and the slopes of linear fits [hole; $a = 0.585 \mu\text{m}\cdot\text{k}\Omega$, electron; $a = 0.680 \mu\text{m}\cdot\text{k}\Omega$] in Fig. 3(f), $a\sigma_{\min}$ is estimated to be 0.257 and 0.299 μm for hole and electron carriers, respectively. These values are in good agreement with the intercepts of the linear fits in Fig. 3(f), 0.293 and 0.285 μm in the hole and electron sides, respectively. Thus, the intercept in the linear fit contains valuable information on both σ_{\min} and Δ_{SO} .

C. Candidate for strong spin relaxation: covalently bonded adsorbates

Covalently bonded adsorbates, charged impurities, and ripples are generally accepted as momentum-scattering sources.²³ A theoretical estimation of Δ_{SO} induced by ripples is on the order of 10^{-5} to 10^{-4} eV,^{9,12} much smaller than our result. First-principle calculations,¹⁴ taking into account scattering by the charged impurities with densities of a few 10^{12} cm^{-2} , also result in τ_s values that are too long (on the order of μs). In contrast, the values of our Δ_{SO} are in fair agreement with the theoretical prediction [a few meV], considering distortion of the graphene lattice from sp^2 to sp^3 by hybridization of adsorbates with carbon atoms.¹⁰ Our σ also shows a good qualitative fit with the resonant scattering²⁴⁻²⁸ from adsorbates. In Fig. 4, the measured σ [for fixed $V_{TG} = -1$ V and varying V_{BG}] and its fit to the following resonant-scattering expression²⁵⁻²⁸ are plotted.

$$\sigma = \frac{2e^2}{\pi h} \frac{1}{\pi n_{\text{ad}}} [q \pm k_F \ln(k_F R)]^2, \quad (5)$$

where n_{ad} , k_F , and R are the density of adsorbates, the Fermi wavevector of carriers [zero at charge-neutral point ($V_{BG} = 5.4$ V)], and the range of scattering potential, respectively. Here, + (−) corresponds to electron-donating (hole-donating) adsorbates. As adopted by a theoretical model by Wehling *et al.*²⁷ a parameter q is introduced in Eq. (5) to fit the asymmetry in the measured σ with respect to the charge-neutral point. A finite q leads to an asymmetry in

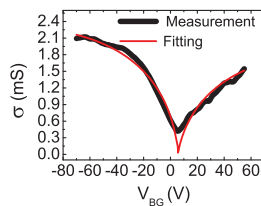


FIG. 4. (Color online) The measured σ for varying V_{BG} with a neutral top-gate [$V_{TG} = -1$ V] and its fit with a resonant scattering model.

σ , where q is finite (zero) if the midgap state forms away from (at) the charge-neutral point. Unlike the midgap states created by vacancies, the midgap states by adsorbates can usually be created away from the charge-neutral point.²⁶⁻²⁸ As the midgap states form further away from the charge-neutral point, the value of q increases and the asymmetry of σ is enhanced.^{27,28} As seen in Fig. 4, with $n_{\text{ad}} = 1.17 \times 10^{11} \text{ cm}^{-2}$ (electron-donating), $q = 3.05 \times 10^5 \text{ cm}^{-1}$, and $R = 0.66 \text{ nm}$, Eq. (5) fits well the measured σ including both the sublinearity and the asymmetry, where quantum mechanical corrections are required to fit σ around the charge-neutral point.^{27,28}

It has been demonstrated that carrier spins can be polarized at the edges of a zigzag graphene nanoribbon,²⁹ which can lead to edge-induced spin relaxation. But, this long-range edge magnetic order is bound to be broken for disordered edges as in our graphene nanoribbon. In fact, no enhancement of the spin relaxation was observed in the graphene ribbons³ as their widths varied in the range of 1 μm –100 nm. But, the formation of clusters of local magnetic moments is still possible, which may relax spins with the rate of $1/\tau_s \sim n_M \nu J^2$, where n_M is the concentration of magnetic moments, and J is the exchange coupling between the magnetic moments and the conduction electrons.³⁰ A simple proportionality relation holds³⁰ between this τ_s and τ_m rather than the ν -dependent scaling relation in Eq. (2). Thus, the spin relaxation observed in our study is not of magnetic origin. Spin relaxation by magnetic impurities or clusters is a subject of high interest by itself and further investigations are required.

Recently, for tunnel-contact devices, a longer λ_s was observed than for direct-contact devices, and the discrepancy was attributed to contact-induced spin relaxation in direct-contact devices.^{4,7} However, the robust scalability between λ_s and σ in Fig. 3(f) is not explained by assuming that contact-induced spin relaxation, in correlation with varying R_c in Fig. 2(d), governs the evolution of λ_s .

Thus, the covalently bonded adsorbates are the most likely spin-relaxing source in diffusive graphene. Recent observations^{7,16} of a longer spin-relaxation time in multilayer graphene than in monolayer graphene is explicable by the reduced scattering rate from the adsorbates on the surface.^{24,25} Enhanced flatness³¹ in multilayer graphene also contributes to the reduced scattering rate.

IV. DISCUSSION ON THE EVOLUTION OF SPIN SIGNAL

For a limited range of our sample parameters,²¹ ΔR_{NL} can be expressed as,¹⁷

$$\Delta R_{\text{NL}} \approx 4p^2 R_n \frac{\frac{R_c^{\text{inj}}}{R_n} \frac{R_c^{\text{det}}}{R_n} e^{-L/\lambda_s}}{\left(1 + 2\frac{R_c^{\text{inj}}}{R_n}\right) \left(1 + 2\frac{R_c^{\text{det}}}{R_n}\right) - e^{-2L/\lambda_s}}, \quad (6)$$

where R_c^{inj} (R_c^{det}) is the contact resistance of the injector (detector), $R_n \equiv \lambda_s/(\sigma w)$ (w ; the width of graphene), and p is the interfacial magnetic polarization. Applying the linear relationship between λ_s and σ in Fig. 3(f) to Eq. (6) for fixed injector (detector) contact resistance [$R_c^{\text{inj(det)}}$] = 1.29 (1.31) $\text{k}\Omega$] and polarization ($p = 0.17$), the resulting ΔR_{NL}

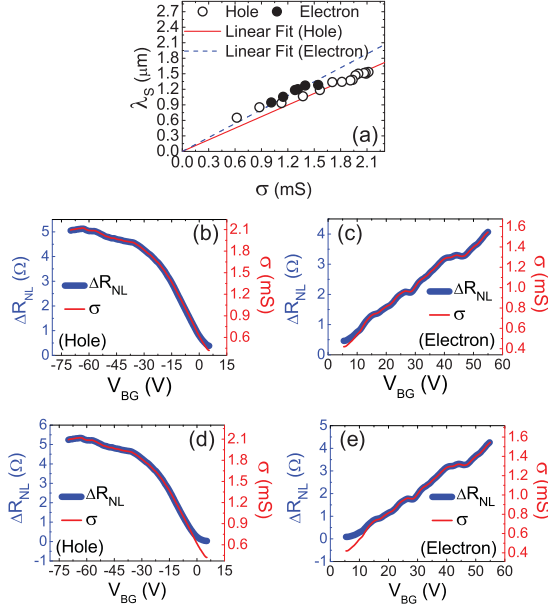


FIG. 5. (Color online) (a) The identical data to Fig. 3(f) but the linear fits with compulsive zero intercept. ΔR_{NL} and σ for (b) hole and (c) electron regions as applying the linear relationship in Fig. 3(f). Similar plots of ΔR_{NL} and σ to (b) and (c) in (d) [hole] and (e) [electron] but as applying the linear relationship in (a).

for varying V_{BG} with a fixed $V_{TG} = -1$ V (neutral top gate) is obtained as in Figs. 5(b) and 5(c) for hole and electron carriers, respectively. Unlike Fig. 2(a), but similar to Figs. 2(b) and 2(c), ΔR_{NL} in Figs. 5(b) and 5(c) traces σ in the entire range of V_{BG} . The scalability between ΔR_{NL} and σ also holds for other values of $R_c^{inj(det)}$ and p . Assuming a constant polarization for a fixed contact resistance,⁶ this supports the description in the Sec. III A that the weak correlation between ΔR_{NL} and σ for varying V_{BG} and fixed $V_{TG} = -1$ V is attributed to the V_{BG} -induced variation of contact resistances.

A linear fit similar to Fig. 3(f) between λ_s and σ but with the constraint of zero intercept is seen in Fig. 5(a). Applying this linear relationship to Eq. (6), the resulting ΔR_{NL} is plotted in Figs. 5(d) and 5(e) for hole and electron carriers, respectively. Since the effect of σ_{min} [finite intercept] is unduly neglected in this case the expected variation of ΔR_{NL} does not go with σ as the charge-neutral point is approached.

In Fig. 6(a), ΔR_{NL} is plotted with the variation of σ , where $\Delta R_{NL}(H)$, $\Delta R_{NL}(E)$, $\Delta R_{NL}(H0)$, and $\Delta R_{NL}(E0)$ are taken from Figs. 5(b), 5(c), 5(d), and 5(e), respectively. An almost-linear relationship in the entire range of σ is seen in $\Delta R_{NL}(H)$ and $\Delta R_{NL}(E)$, while a growing deviation from linearity near the charge-neutral point is seen in $\Delta R_{NL}(H0)$, $\Delta R_{NL}(E0)$, again due to neglecting σ_{min} .

In Fig. 6(b) the evolution of ΔR_{NL} is traced for different values of λ_s with fixed $R_c^{inj(det)} = 1.29(1.31)$ k Ω and $p = 0.17$, where λ_s decreases monotonously by 10% while the linear relationship in Fig. 3(f) between λ_s and σ is retained. It demonstrates the sensitive nature of ΔR_{NL} to the variation of λ_s , which is attributed to the exponential factor in the numerator of Eq. (6).

In Figs. 6(c) and 6(d), ΔR_{NL} is plotted with varying σ (corresponding to the variation in V_{TG} at fixed $V_{BG} = -40$

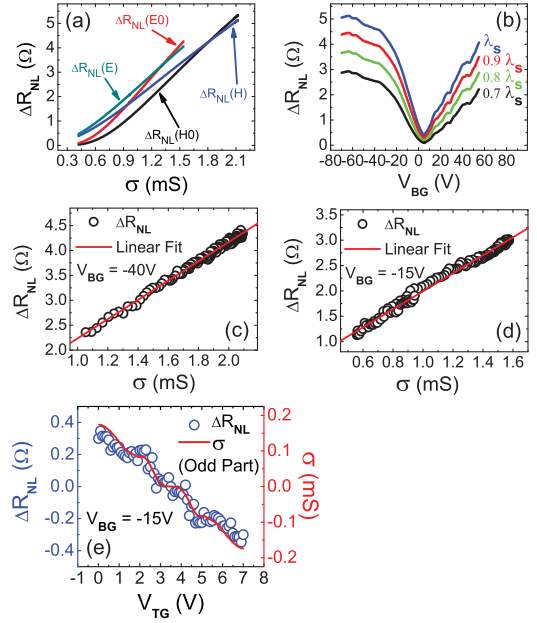


FIG. 6. (Color online) (a) $\Delta R_{NL}(H)$, $\Delta R_{NL}(E)$, $\Delta R_{NL}(H0)$, and $\Delta R_{NL}(E0)$ for varying σ [varying V_{BG} at fixed $V_{TG} = -1$ V] are taken from Figures 5(b), 5(c), 5(d), and 5(e), respectively. (b) ΔR_{NL} for different λ_s with fixed $R_c^{inj(det)} = 1.29(1.31)$ k Ω and $p = 0.17$. ΔR_{NL} for varying σ [varying V_{TG}] and the corresponding linear fit at (c) $V_{BG} = -40$ V and (d) $V_{BG} = -15$ V, with the data taken from Figs. 2(b) and 2(c), respectively. (e) The odd parts of ΔR_{NL} and σ to the charge-neutral point of top-gate ($V_{TG} = 3.5$ V) at $V_{BG} = -15$ V for varying V_{TG} .

and -15 V, respectively), where the data are taken from Figs. 2(b) and 2(c). The robustness of the linear relationship between ΔR_{NL} and σ , even in an electric field that is present at an edge of the top gate, is very similar to that of Fig. 6(a) [$\Delta R_{NL}(H)$ and $\Delta R_{NL}(E)$] for a neutral top gate. In particular, in Fig. 6(d), it is notable that the linear relationship stays valid as carriers traverse the bipolar configuration, where σ is in the range between 0.64 and 1.09 mS [see also Fig. 2(c)]. Since ΔR_{NL} is very sensitive to the variation in λ_s as in Fig. 6(b), the observed linear relationship can hardly hold if an abrupt spin relaxation occurs by the interfacial electric field. Thus, our analysis indicates that no further relaxation of the spin state is induced by the presence of the potential-varying interface, either unipolar or bipolar, in graphene at least in a diffusive limit at 4.2 K as used in this study. In Fig. 6(e), in order to extract the effect of p-n interface,³² odd parts of ΔR_{NL} and σ with respect to the charge-neutral point of top gate ($V_{TG} = 3.5$ V) at $V_{BG} = -15$ V are plotted for varying V_{TG} . The scalability between ΔR_{NL} and σ is robust to the presence of bipolar interface, i.e., the occurrence of Klein tunneling. This leads to a conclusion that Klein tunneling itself does not induce any notable spin relaxation in our study.

V. CONCLUSION

In a nonlocal spin-valve device consisting of a diffusive graphene layer, the spin signal is controlled precisely in conformation with the top-gate-induced conductivity variation.

The spin state is most likely relaxed by covalently bonded adsorbates via the EY mechanism. But, the spin transport is not affected by the presence of either unipolar or bipolar potential interface. Accounting for the density-dependent factor ν^2 in the relationship between the spin and momentum relaxation times, arising from the unique linear dispersion relation of graphene, is crucial to correctly identifying the spin-relaxation mechanism in graphene.

ACKNOWLEDGMENTS

H.J.L. is grateful to Hyun-Woo Lee for critical reading of the manuscript and valuable inputs. H.J.L. was supported by National Research Foundation of Korea (NRF) through Acceleration Research Grant No. R17-2008-007-01001-0 and Grant No. 2009-0083380. S.K. was supported by WCU (World Class University) program (Division of Advanced Materials Science, POSTECH) of NRF through R31-2008-000-10059-0.

*Current address: DPMC and GAP, University of Geneva, 24 quai Ernest-Ansermet, 1211 Geneva, Switzerland

†hjlee@postech.ac.kr

- ¹N. Tombros, C. Jozsa, M. Popinciuc, H. T. Jonkman, and B. J. van Wees, *Nature (London)* **448**, 571 (2007).
- ²W. Han, K. Pi, W. Bao, K. M. McCreary, Y. Li, W. H. Wang, C. N. Lau, and R. K. Kawakami, *Appl. Phys. Lett.* **94**, 222109 (2009).
- ³M. Popinciuc, C. Jozsa, P. J. Zomer, N. Tombros, A. Veligura, H. T. Jonkman, and B. J. van Wees, *Phys. Rev. B* **80**, 214427 (2009).
- ⁴W. Han, K. Pi, K. M. McCreary, Y. Li, J. J. I. Wong, A. G. Swartz, and R. K. Kawakami, *Phys. Rev. Lett.* **105**, 167202 (2010).
- ⁵N. Tombros, S. Tanabe, A. Veligura, C. Jozsa, M. Popinciuc, H. T. Jonkman, and B. J. van Wees, *Phys. Rev. Lett.* **101**, 046601 (2008).
- ⁶C. Józsa, T. Maassen, M. Popinciuc, P. J. Zomer, A. Veligura, H. T. Jonkman, and B. J. van Wees, *Phys. Rev. B* **80**, 241403(R) (2009).
- ⁷W. Han and R. K. Kawakami, e-print arXiv:1012.3435.
- ⁸K. Pi, W. Han, K. M. McCreary, A. G. Swartz, Y. Li, and R. K. Kawakami, *Phys. Rev. Lett.* **104**, 187201 (2010).
- ⁹D. Huertas-Hernando, F. Guinea, and A. Brataas, *Phys. Rev. Lett.* **103**, 146801 (2009).
- ¹⁰A. H. Castro Neto and F. Guinea, *Phys. Rev. Lett.* **103**, 026804 (2009).
- ¹¹H. Min, J. E. Hill, N. A. Sinitsyn, B. R. Sahu, L. Kleinman, and A. H. MacDonald, *Phys. Rev. B* **74**, 165310 (2006); D. Huertas-Hernando, F. Guinea, and A. Brataas, *ibid.* **74**, 155426 (2006); Y. Yao, F. Ye, X.-L. Qi, S.-C. Zhang, and Z. Fang, *ibid.* **75**, 041401(R) (2007).
- ¹²M. Gmitra, S. Konschuh, C. Ertler, C. Ambrosch-Draxl, and J. Fabian, *Phys. Rev. B* **80**, 235431 (2009).
- ¹³I. Žutić, J. Fabian, and S. Das Sarma, *Rev. Mod. Phys.* **76**, 323 (2004).
- ¹⁴C. Ertler, S. Konschuh, M. Gmitra, and J. Fabian, *Phys. Rev. B* **80**, 041405(R) (2009).
- ¹⁵P. R. Wallace, *Phys. Rev.* **71**, 622 (1947).
- ¹⁶T. Maassen, F. K. Dejene, M. H. D. Guimarães, C. Józsa, and B. J. van Wees, *Phys. Rev. B* **83**, 115410 (2011); T.-Y. Yang *et al.*, e-print arXiv:1012.1156.
- ¹⁷S. Takahashi and S. Maekawa, *Phys. Rev. B* **67**, 052409 (2003).
- ¹⁸T. Kimura, Y. Otani, and J. Hamrle, *Phys. Rev. B* **73**, 132405 (2006).
- ¹⁹J. R. Williams, L. DiCarlo, and C. M. Marcus, *Science* **317**, 638 (2007); D.-K. Ki and H.-J. Lee, *Phys. Rev. B* **79**, 195327 (2009); D.-K. Ki, S.-G. Nam, H.-J. Lee, and B. Özyilmaz, *ibid.* **81**, 033301 (2010).
- ²⁰R. Nouchi, M. Shiraishi, and Y. Suzuki, *Appl. Phys. Lett.* **93**, 152104 (2008); B. Huard, N. Stander, J. A. Sulpizio, and D. Goldhaber-Gordon, *Phys. Rev. B* **78**, 121402(R) (2008); P. Blake *et al.*, *Solid State Commun.* **149**, 1068 (2009); S. Russo, M. F. Craciun, M. Yamamoto, A. F. Morpurgo, and S. Tarucha, *Physica E* **42**, 677 (2010).
- ²¹The sample parameters are in the range of $3.57 \text{ k}\Omega \leq R_n \leq 5.24 \text{ k}\Omega$, $0.95 \text{ k}\Omega \leq R_c \leq 1.56 \text{ k}\Omega$, and $R_f \approx 0.22 \Omega$. Here, $R_n \equiv \lambda_s/(\sigma w)$ (w ; the width of graphene), $R_f \equiv \lambda_f/(\sigma_f A_f)$ [λ_f ($= 36 \text{ nm}$) and σ_f ($= 7.3 \times 10^6 \Omega^{-1}\text{m}^{-1}$) are the spin relaxation length and the conductivity in a ferromagnet; A_f is the contact area in the ferromagnet and graphene]. Therefore, our sample is in the intermediate regime defined in Ref. 17, but with a non-negligible value of R_c/R_n . F. J. Jedema, M. S. Nijboer, A. T. Filip, and B. J. van Wees, *Phys. Rev. B* **67**, 085319 (2003).
- ²²M. Johnson and R. H. Silsbee, *Phys. Rev. B* **37**, 5312 (1988); F. J. Jedema, H. B. Heersche, A. T. Filip, J. J. A. Baselmans, and B. J. van Wees, *Nature (London)* **416**, 713 (2002); G. Mihajlović, J. E. Pearson, S. D. Bader, and A. Hoffmann, *Phys. Rev. Lett.* **104**, 237202 (2010).
- ²³N. M. R. Peres, *Rev. Mod. Phys.* **82**, 2673 (2010).
- ²⁴M. Monteverde *et al.*, *Phys. Rev. Lett.* **104**, 126801 (2010); Z. H. Ni *et al.*, *Nano Lett.* **10**, 3868 (2010).
- ²⁵V. M. Pereira, F. Guinea, J. M. B. Lopes dos Santos, N. M. R. Peres, and A. H. Castro Neto, *Phys. Rev. Lett.* **96**, 036801 (2006); J. P. Robinson, H. Schomerus, L. Oroszlány, and V. I. Fal'ko, *ibid.* **101**, 196803 (2008); T. Stauber, N. M. R. Peres, and F. Guinea, *Phys. Rev. B* **76**, 205423 (2007).
- ²⁶T. O. Wehling, M. I. Katsnelson, and A. I. Lichtenstein, *Phys. Rev. B* **80**, 085428 (2009).
- ²⁷T. O. Wehling, S. Yuan, A. I. Lichtenstein, A. K. Geim, and M. I. Katsnelson, *Phys. Rev. Lett.* **105**, 056802 (2010).
- ²⁸A. Ferreira, J. Viana-Gomes, Johan Nilsson, E. R. Mucciolo, N. M. R. Peres, and A. H. Castro Neto, *Phys. Rev. B* **83**, 165402 (2011).
- ²⁹Y.-W. Son, M. L. Cohen, and S. G. Louie, *Nature (London)* **444**, 347 (2006).
- ³⁰P. Wenk and S. Kettemann, e-print arXiv:1012.3575.
- ³¹D. C. Elias *et al.*, *Science* **323**, 610 (2009).
- ³²B. Huard, J. A. Sulpizio, N. Stander, K. Todd, B. Yang, and D. Goldhaber-Gordon, *Phys. Rev. Lett.* **98**, 236803 (2007).